Article

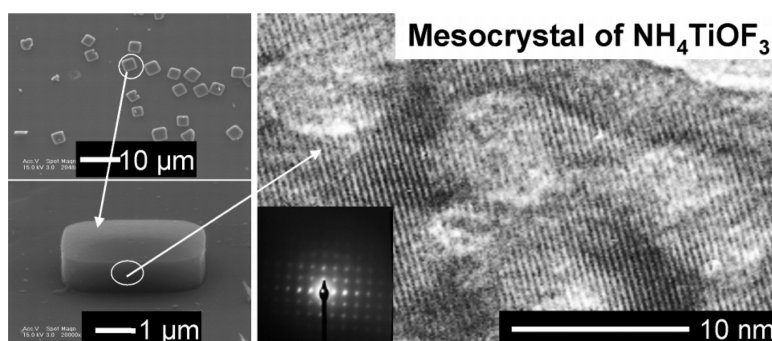# A Facile Synthesis of Uniform NHTiOF Mesocrystals and Their Conversion to TiO Mesocrystals

Lei Zhou, David Smyth-Boyle, and Paul O'Brien

More About This Article

Additional resources and features associated with this article are available within the HTML version:

- Supporting Information
- Links to the 2 articles that cite this article, as of the time of this article download
- Access to high resolution figures
- Links to articles and content related to this article
- Copyright permission to reproduce figures and/or text from this article

View the Full Text HTML

A Facile Synthesis of Uniform NH$_4$TiOF$_3$ Mesocrystals and Their Conversion to TiO$_2$ Mesocrystals

Lei Zhou, David Smyth-Boyle, and Paul O'Brien*

School of Chemistry and Manchester Materials Science Centre, University of Manchester, Oxford Road, Manchester, M13 9PL, United Kingdom

Received August 16, 2007; E-mail: paul.obrien@manchester.ac.uk

Abstract: Uniform mesocrystals of TiO$_2$ (anatase) have been prepared from mesocrystals of NH$_4$TiOF$_3$. NH$_4$TiOF$_3$ was synthesized from an aqueous solution containing (NH$_4$)$_2$TiF$_6$ and H$_3$BO$_3$ in the presence of a nonionic surfactant Brij 56, Brij 58, or Brij 700, at low temperatures. The exterior shapes of NH$_4$TiOF$_3$ mesocrystals can be tuned by adjusting the reagent concentration, reaction time, reaction temperature, and rate of stirring. The formation of the NH$_4$TiOF$_3$ mesocrystals proceeds via a self-assembly process involving nonclassical crystal growth. By sintering in air at 450 °C, or washing with H$_3$BO$_3$ solution at ambient temperatures, the NH$_4$TiOF$_3$ mesocrystals can be converted to mesocrystals of TiO$_2$ (anatase), and the original architecture is retained.

Introduction

The organization of matter across different multiple length scales is ubiquitous in nature and well-exampled by biomaterials.[1,2] Monodisperse spherical particles with sizes ranging from a few nanometers (e.g., quantum dots) to a few micrometers (i.e., conventional colloidal particles) can be used to form more macroscopic assemblies.[3-7] For example, nanosized semiconductor or metal particles with core–shell structures have been used to construct nanocrystal superlattices;[3-5] microsized SiO$_2$ and polystyrene colloidal particles have assembled into photonic crystals.[6] Monodisperse particles with nonspherical shapes can also be used to build novel forms of materials, e.g., cubic zeolite[8,9] or lead zirconate titanate (PZT)[7] particles have been prepared and arranged into single-crystal-like films on glass substrates. In the presence of well-organized templates (such as lyotropic liquid crystal phases of surfactants and colloidal crystals of polystyrene or silica), nanoparticles with irregular shapes and sizes can construct to give an ordered porous structure where the pores can vary from a few nanometers to a few micrometers.[10,11]

Recently, the term "mesocrystal", a new concept describing crystallographically ordered assemblies of nanocrystals was proposed by Cölfen et al.[12] In comparison with ordered suprastructures which emphasize good-ordering between building blocks (or templates) and therefore require very uniform subunits, mesocrystals put more emphasis on crystallographically oriented alignment of subunits, which can result in a single-crystal-like diffraction and do not require regular shapes of subunits.[12-16] In fact, there are no strict distinctions among these types of ordered architectures. The terms emphasize different aspects of a material. For example, although most nanocrystal superlattices (or supracrystals) are crystallographically random, a few papers have reported that nanocrystal superlattices can be crystallographically oriented;[17-19] ordered mesoporous materials can also have well-crystalline walls.[20] In both cases, the higherarchical materials possess the typical property of mesocrystals. Another thing that should be noted is that the term "mesocrystal" has been used previously in literature referring to different concepts.[21-24] In the present paper, the term "mesocrystal" always refers to Cölfen's definition.[12]

Although a few papers have reported on the formation of mesocrystals, the general mechanisms for their formation are

(1) Mann, S. *Biomineralization: Principles and concepts in bioinorganic materials chemistry*; Oxford University Press: Oxford, 2002.
(2) Mann, S. *Biomimetic Materials Chemistry*; John Wiley & Sons: New York, 1997.
(3) Murray, C. B.; Kagan, C. R.; Bawendi, M. G. *Science* **1995**, *270*, 1335.
(4) Redl, F. X.; Cho, K. S.; Murray, C. B.; O'Brien, S. *Nature* **2003**, *423*, 968.
(5) Murray, C. B.; Kagan, C. R.; Bawendi, M. G. *Annu. Rev. Mater. Sci.* **2000**, *30*, 545.
(6) Xia, Y. N.; Gates, B.; Yin, Y. D.; Lu, Y. *Adv. Mater.* **2000**, *12*, 693.
(7) Liu, X. Y.; McCandlish, E. F.; McCandlish, L. E.; Mikulka-Bolen, K.; Ramesh, R.; Cosandey, F.; Rossetti, G. A.; Riman, R. E. *Langmuir* **2005**, *21*, 3207.
(8) Ha, K.; Lee, Y. J.; Jung, D. Y.; Lee, J. H.; Yoon, K. B. *Adv. Mater.* **2000**, *12*, 1614.
(9) Lee, J. S.; Ha, K.; Lee, Y. J.; Yoon, K. B. *Adv. Mater.* **2005**, *17*, 837.
(10) Yang, P. D.; Zhao, D. Y.; Margolese, D. I.; Chmelka, B. F.; Stucky, G. D. *Nature* **1998**, *396*, 152.
(11) Wijnhoven, J. E. G. J.; Vos, W. L. *Science* **1998**, *281*, 802.

(12) Cölfen, H.; Antonietti, M. *Angew. Chem., Int. Ed.* **2005**, *44*, 5576.
(13) Cölfen, H.; Yu, S. H. *MRS Bull.* **2005**, *30*, 727.
(14) Cölfen, H.; Mann, S. *Angew. Chem., Int. Ed.* **2003**, *42*, 2350.
(15) Niederberger, M.; Cölfen, H. *Phys. Chem. Chem. Phys.* **2006**, *8*, 3271.
(16) Zhou, L.; Boyle, D. S.; O'Brien, P. *Chem. Commun.* **2007**, 144.
(17) Dumestre, F.; Chaudret, B.; Amiens, C.; Renaud, P.; Fejes, P. *Science* **2004**, *303*, 821.
(18) Soulantica, K.; Maisonnat, A.; Fromen, M. C.; Casanove, M. J.; Chaudret, B. *Angew. Chem., Int. Ed.* **2003**, *42*, 1945.
(19) Nikoobakht, B.; Wang, Z. L.; El-Sayed, M. A. *J. Phys. Chem. B* **2000**, *104*, 8635.
(20) Brezesinski, T.; Groenewolt, M.; Pinna, N.; Amenitsch, H.; Antonietti, M.; Smarsly, B. M. *Adv. Mater.* **2006**, *18*, 1827.
(21) Allahyarov, E.; Löwen, H.; Gompper, G. *Europhys. Lett.* **2004**, *68*, 894.
(22) Huang, J. P. *Phys. Rev. E* **2004**, *70*, 5.
(23) Yamada, K.; Kohiki, S. *Physica E* **1999**, *4*, 228.
(24) Ko, C. H.; Kim, J. M.; Ryoo, R. *Microporous Mesoporous Mater.* **1998**, *21*, 235.

still largely unexplored.[12] In most cases, mesocrystals exist as intermediates of crystallization. Their syntheses provide a challenge to accepted views on crystal growth[25] as typically described by a process of nucleation and growth and/or subsequent Ostwald ripening. Moreover, by using low temperature soft-chemical routes, these systems may also offer a paradigm to mimic assembly processes that govern the formation of many biological inorganic materials.[14] In the present work, a soft chemical solution method has been employed to synthesize uniform NH_4TiOF_3 mesocrystals. The growth process is detailedly investigated by a high-resolution TEM technique, and a three-step mechanism is proposed.

Titanium dioxide has been extensively studied because of its wide variety of practical applications, including uses in photocatalysis,[26−29] amphiphilic coating,[30] and dye-sensitized solar cells.[31,32] A variety of TiO_2 nanomaterials have been prepared including spheres,[33−35] porous films,[10,11] nanofibers,[36] nanowires,[37] and nanotubes.[38] Although monodisperse spherical TiO_2 particles have been extensively studied and used to make colloidal crystals,[33] there are few reports reporting a reproducible synthesis of TiO_2 particles with a regular shape and uniform size. In the present work, uniform NH_4TiOF_3 mesocrystals were converted to anatase TiO_2 by an oriented transformation on sintering in air at 450 °C or washing with H_3BO_3 solution at ambient temperatures, retaining the unique mesocrystal aspect.

Experimental Section

Preparation of NH_4TiOF_3 Mesocrystals. Typical reaction conditions for the preparation of mesocrystalline NH_4TiOF_3 particles were as follows: A nonionic surfactant (7.5 g of Brij 56, 15 g of Brij 58, or 10 g of Brij 700) was added to a freshly prepared 50 cm^3 of solution containing $(NH_4)_2TiF_6$ (0.1 mol $dm^{−3}$) and H_3BO_3 (0.2 mol $dm^{−3}$). "Brij" is a registered trademark of ICI Americas, Inc. Brij series surfactants are polyoxyethylene fatty ethers and are composed of a hydrophilic polyoxyethylene chain and a hydrophobic polyether chain. The molecular formulas are $C_{16}H_{33}(OCH_2CH_2)_{10}OH$ for Brij 56, $C_{16}H_{33}(OCH_2CH_2)_{20}OH$ for Brij 58, and $C_{18}H_{37}(OCH_2CH_2)_{100}OH$ for Brij 700. Stirring was stopped after the surfactant was completely dispersed. The solution was then kept at 35 °C for 20 h. Precipitates were collected, separated by centrifugation and washed (×3) sequentially with DI water, ethanol, and acetone.

Preparation of TiO_2 Mesocrystals. Two different routes were used to convert the mesocrystals of NH_4TiOF_3 to mesocrystalline TiO_2. First, mesocrystals of NH_4TiOF_3 were heated at 450 °C for 2 h in air. Second, mesocrystals of NH_4TiOF_3 were placed in a H_3BO_3 solution (0.5 mol $dm^{−3}$) with moderate stirring at 35 °C or 60 °C for up to 4 h; washed particles were collected and cleaned by consecutive centrifuging, decanting, and redispersing, in water (twice) and then in ethanol (twice).
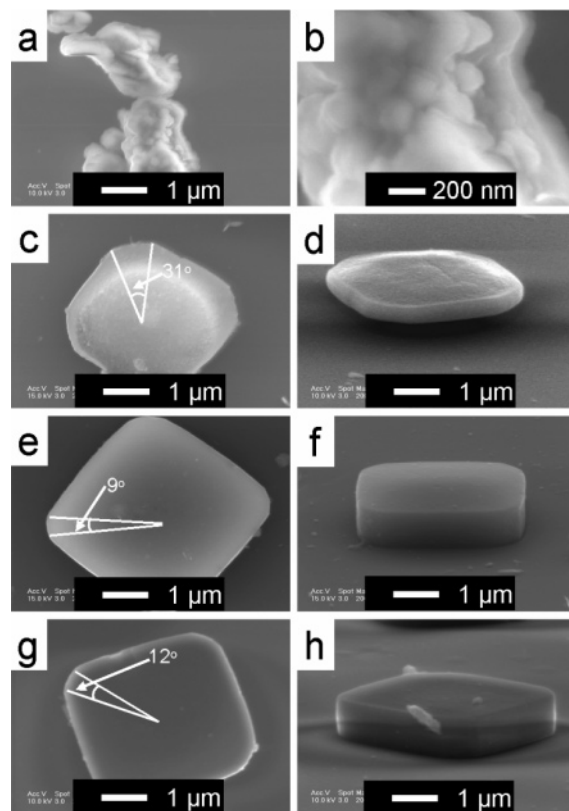
(25) Pileni, M. P. *Nanocrystals forming mesoscopic structures*; Wiley-VCH: Weinheim, Germany, 2005.
(26) Nozik, A. J. *Nature* **1975**, *257*, 383.
(27) Khan, S. U. M.; Al-Shahry, M.; Ingler, J. W. B. *Science* **2002**, *297*, 2243.
(28) Fujihira, M.; Satoh, Y.; Osa, T. *Nature* **1981**, *293*, 206.
(29) Asahi, R.; Morikawa, T.; Ohwaki, T.; Aoki, K.; Taga, Y. *Science* **2001**, *293*, 269.
(30) Wang, R.; Hashimoto, K.; Fujishima, A.; Chikuni, M.; Kojima, E.; Kitamura, A.; Shimohigoshi, M.; Watanabe, T. *Nature* **1997**, *388*, 431.
(31) O'Regan, B.; Grätzel, M. *Nature* **1991**, *353*, 737.
(32) Bach, U.; Lupo, D.; Comte, P.; Moser, J. E.; Weissörtel, F.; Salbeck, J.; Spreitzer, H.; Grätzel, M. *Nature* **1998**, *395*, 583.
(33) Jiang, X. C.; Herricks, T.; Xia, Y. N. *Adv. Mater.* **2003**, *15*, 1205.
(34) Li, Y. L.; Ishigaki, T. *Chem. Mater.* **2001**, *13*, 1577.
(35) Caruso, R. A.; Susha, A.; Caruso, F. *Chem. Mater.* **2001**, *13*, 400.
(36) Li, D.; Xia, Y. N. *Nano Lett.* **2003**, *3*, 555.
(37) Penn, R. L.; Banfield, J. F. *Science* **1998**, *281*, 969.
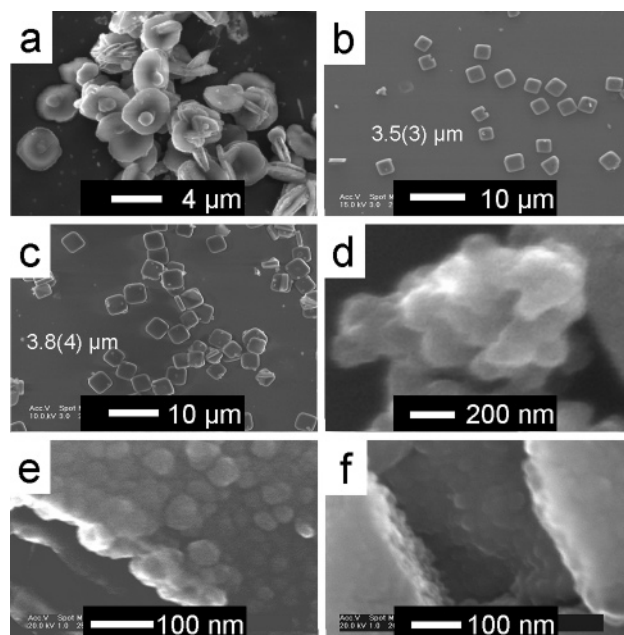(38) Lee, J. H.; Leu, I. C.; Hsu, M. C.; Chung, Y. W.; Hon, M. H. *J. Phys. Chem. B* **2005**, *109*, 13056.

Figure 1. Low and high magnification SEM images of a sample prepared (a and b) without surfactant. Top and cross-sectional views of samples prepared with (c and d) Brij 56, (e and f) Brij 58, or (g and h) Brij 700.

Characterization. Scanning electron micrographs (SEM) were obtained using a Philips XL30 FEG SEM or JEOL JMS-6300 SEM. Prior to analysis, samples were carbon- (or gold-)coated using an Edwards Sputter Coater (E306A for carbon coating, S150B for gold coating). Powder X-ray diffraction studies were performed using a Bruker AXS D8 diffractometer over values of 2θ from 5° to 90°. Transmission electron microscopy (TEM) was performed using a Philips CM 200 (200 kV) instrument, with video images recorded using a Kodak Easyshare CX7430 digital camera. For some experiments, a FEI Tecnai F30 FEGTEM (300 kV) microscope was employed. A Seiko SSC/S200 instrument was employed for TGA using a heating rate of 5 °C $min^{−1}$ in air. Elemental analysis was performed at the University of Manchester microanalytical laboratory using a Carlo Erba CHNS−O EA1108 Elemental Analyzer for C, H, and N and a Fisons Horizon Elemental Analysis ICP-OED spectrometer for B and Ti.

Results and Discussion

Characterization of Samples Synthesized in the Presence of Different Surfactants. SEM images of samples synthesized under the typical conditions (for details see Experimental Section) are shown in Figure 1. The sample prepared without surfactant gave irregular aggregates (Figure 1a) composed of small grains of size ∼150 nm (Figure 1b). The samples prepared with Brij 58 ($C_{16}H_{33}(OCH_2CH_2)_{20}OH$) or Brij 700 ($C_{18}H_{37}(OCH_2CH_2)_{100}OH$)) gave well-facetted polyhedral particles. These particles can be seen as platelets (the difference between shorter and longer edge lengths was less than 5%), with a defined thickness and smoothly truncated corners (Figure 1e−h). Almost all particles have uniform shapes and sizes, as clearly shown in the low magnification SEM images (Figure 2b and c). The mean edge length and thickness of the Brij 58 sample are 3.5(3) μm and 0.78(9) μm, respectively (for the Brij 700 sample, 3.8(4) μm and 0.92(8) μm, respectively). High

$\qquad$

Figure 2. Low magnification SEM images of typical samples prepared with (a) Brij 56, (b) Brij 58, or (c) Brij 700. High magnification SEM images of the samples prepared with (d) Brij 56 or (e and f) Brij 58.
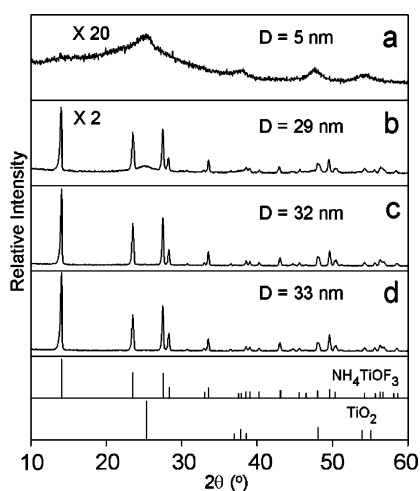

Figure 3. Powder XRD (p-XRD) patterns and average crystallite sizes (D, calculated using Scherrer Equation) for samples prepared (a) without surfactant and with surfactants: (b) Brij 56, (c) Brij 58, or (d) Brij 700. (TiO_2 from JCPDS 86−1156; NH_4TiOF_3 from ref 39.)

magnification SEM images of a typical, regular particle isolated from the Brij 58 sample are shown in Figure 2e and f. Particles with sizes of 20∼40 nm are clearly visible, not only on the surface but within the interior, indicating that these materials are composed of smaller grains. For the sample prepared with Brij 56, both irregular aggregates (Figure 2d, similar to the sample prepared without surfactant) and well-facetted polyhedral particles (Figure 1c and d, similar to the samples prepared with Brij 58 or Brij 700) were obtained (Figure 2a). In comparison to the samples prepared with Brij 58 or Brij 700, the regular particles presented in the Brij 56 sample are thinner, possess convex upper/lower faces, and have more round corners.

Powder XRD patterns (p-XRD, Figure 3) indicate that the main component of a sample prepared without surfactant is nanocrystalline anatase TiO_2, while samples prepared with surfactants (Brij 56, Brij 58, or Brij 700) are mainly composed
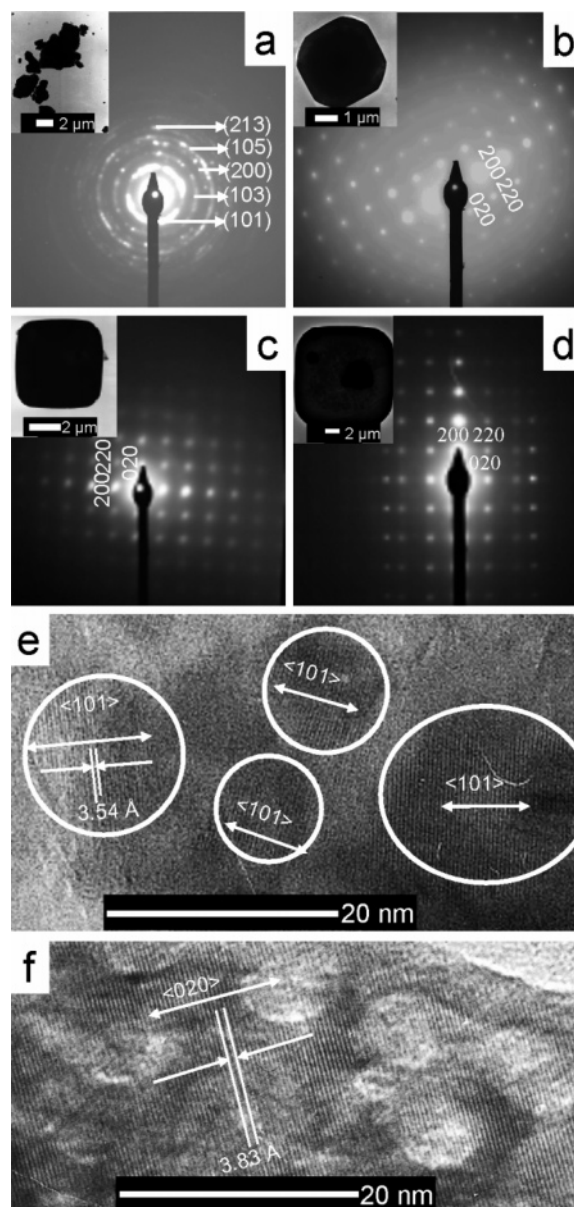

Figure 4. Low magnification TEM images and SAED patterns of typical samples prepared (a) without surfactant or with surfactants: (b) Brij 56, (c) Brij 58, or (d) Brij 700. High magnification TEM images of the samples prepared (e) without surfactant and (f) with Brij 58.

Table 1. Results of Element Analysis and Estimated Components of Samples Prepared under Typical Conditions[a]

surfactants used	Ti (%)	H (%)	N (%)	C (%)	B (%)	NH₄TiOF₃ (%)
no surfactant	46.07	1.56	N/A	1.34	<0.1	N/A
Brij 56	37.45	2.21	6.06	0.33	0.30	60.12
Brij 58	33.56	2.93	9.44	<0.30	1.04	93.64
Brij 700	33.20	2.85	9.17	<0.30	0.76	90.97

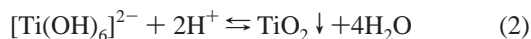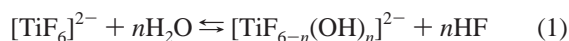[a] For details, see Experimental Section. N/A = not applicable.

of crystalline NH_4TiOF_3. The weak reflection at ∼25° (2θ) indexed to the (101) reflection of anatase TiO_2 is also apparent in the p-XRD pattern of the Brij 56 sample (Figure 3b). The SEM images (shown in Figure 1 and Figure 2) and average crystallite sizes (D, calculated using the Scherrer Equation and shown in Figure 3) lead to the conclusion that the irregular aggregates characterized in the samples prepared without surfactant or with Brij 56 are composed of TiO_2 nanocrystallites

with dimensions of ∼5 nm, while regular particles presented in the samples prepared with surfactants (Brij 56, Brij 58, or Brij 700) are composed of NH_4TiOF_3 nanocrystallites with a critical dimension of ∼30 nm. Nanocrystallites of NH_4TiOF_3 are clearly visible in high magnification SEM images (Figure 2e and f). Elemental analyses are summarized and listed in Table 1 (for details see Supporting Information) and are consistent with the p-XRD studies (Figure 3).
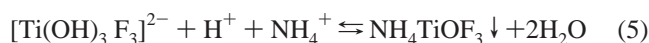
TEM images and SAED patterns of the samples are shown in Figure 4. For the sample prepared with Brij 56, irregular aggregates of anatase are obtained. The concentric diffraction rings of the SAED pattern (Figure 4a) demonstrate the polycrystalline character of these particles. HR-TEM images (Figure 4e) indicate that these irregular aggregates are composed of crystallographically disordered nanocrystalline anatase with dimensions of 5∼10 nm. These critical dimensions are consistent with the dimensions calculated using the Scherrer Equation (Figure 3).

The regular particles in the samples prepared with Brij 56, Brij 58, or Brij 700 were also investigated by HR-TEM and similar results obtained. A high magnification TEM image of the Brij 58 sample is shown in Figure 4f. The regions of low contrast between individual crystallites indicate that mesopores (or interstitial regions) with dimensions of 2∼5 nm are present in the particle. The walls surrounding pores are constructed of nanocrystals, whose lengths extend to 25 nm or more, in agreement with the average crystallite sizes calculated from the diffraction data (Figure 3). SAED patterns (Figure 4b, c, and d) from regular particles show "single-crystal-like" diffraction with minor distortion. The distortions come from small mismatches between boundaries of the small particles, typical for mesocrystals.[12] Examination of the spatial arrangement of the spots in the SAED patterns shows that the lattice planes giving rise to these spots derives from NH_4TiOF_3 orthorhombic single crystal oriented along the [001] axis.

On the basis of all the results, it is concluded that with no surfactant present nanocrystalline anatase is produced. The solution chemistry of the process has been detailed elsewhere;[40] briefly, nanocrystalline anatase TiO_2 particles are produced via the following processes:

$$[TiF_6]^{2-} + nH_2O \rightleftharpoons [TiF_{6-n}(OH)_n]^{2-} + nHF \quad (1)$$

$$[Ti(OH)_6]^{2-} + 2H^+ \rightleftharpoons TiO_2\downarrow + 4H_2O \quad (2)$$

$$H_3BO_3 + 4HF \rightleftharpoons H^+ + BF_4^- + 3H_2O \quad (3)$$

Boric acid (H_3BO_3) behaves as a fluoride scavenger and consumes excess F^- ions. In the present study, when surfactants are present, the hydrolysis of $[TiF_6]^{2-}$ does not go to completion, but a stable intermediate (NH_4TiOF_3) is obtained because of the presence of oxyethylene (EO) functionalities of the surfactants, which hinder the hydrolysis of the titanium (IV) ions. Possible reactions include

$$[TiF_6]^{2-} + 3H_2O \rightleftharpoons [TiF_3(OH)_3]^{2-} + 3H^+ + 3F^- \quad (4)$$

$$[Ti(OH)_3 F_3]^{2-} + H^+ + NH_4^+ \rightleftharpoons NH_4TiOF_3\downarrow + 2H_2O \quad (5)$$

Growth Processes of the NH_4TiOF_3 Mesocrystals. To obtain more information about the growth processes of the NH_4TiOF_3 mesocrystals, samples were collected and investigated after different reaction times during the preparation of typical sample with Brij 58 (for details see Experimental Section). Results indicate that 2 h of reaction time is sufficient for the formation of small mesocrystals (Figure 5a and b); longer reaction times increase the particle size, but do not alter the basic shape. After 16 h, the small mesocrystals mature to their final size and shape. In comparison to mesocrystals collected after 2 h (Figure 5a and b), mesocrystals obtained over longer periods (such as 8 h, Figure 5c and d) have a smaller curvature at corners due to further growth. This is consistent with an increase in the "growth velocity" toward each corner.

Powder XRD patterns for samples collected after different reaction times are shown in Figure 5e, which indicates that the sample after 50 min is a mixture of crystalline NH_4TiOF_3, $(NH_4)_2TiOF_4$, and $(NH_4)_2TiF_6$; samples after ≥2 h are in contrary mainly composed of NH_4TiOF_3. As the reaction time increases from 50 min to 16 h, average crystallite sizes (D, calculated using the Scherrer Equation) of NH_4TiOF_3 remain almost constant (Figure 5e), suggesting that the nanocrystallites that comprise the final mesocrystals formed at very early stage. As the reaction continues, these primary nanocrystallites remain the same size, but the size of the product mesocrystals increased. This observation suggests that the increased dimensions of the mesocrystals derive from controlled aggregation of smaller nanocrystallites rather than typical ion-by-ion growth processes.[12]

Apparently the early stages (i.e., <2 h) of the crystal growth process are more complex and also probably particularly important in determining the final outcome of the experiment. It is difficult to isolate material during the first 20 min because of its fragile nature and the small amount of material formed. TEM samples for this period were prepared by placing a drop of the initial solution on a carbon-coated copper grid and then allowing it to dry after wicking away the excess solvent with filter paper[41](images are shown in Figure 6a,b). After 5 min of reaction, the solution changed from clear to cloudy. Small rounded particles are present throughout (Figure 6a), which have diameters of the order 60 nm (left inset of Figure 6a). On exposure to the electron beam in the TEM (200 kV), decomposition of material occurs, which is probably consistent with loss of excess surfactant. The SAED pattern (right inset of Figure 6a) from remaining matter shows no evidence for crystallinity. If this cloudy solution (obtained after 5 min) is diluted with water, an apparently homogeneous clear solution is formed. This observation that these small particles are readily redispersed is consistent with an inorganic−organic hybrid structure.

A typical particle after 20 min reaction is shown in Figure 6b, in which some wormlike spacings exist. The widths of these spacing are about 5 nm, close to twice the length of the polyether chain (2.2 nm) of Brij 58 ($C_{16}H_{33}(OCH_2CH_2)_{20}OH$).[42] The measured distance between lattice lines is 6.56 Å. A "single-crystal-like" diffraction with minor distortions, indicative of a

(39) Laptash, N. M.; Maslennikova, I. G.; Kaidalova, T. A. *J. Fluor. Chem.* **1999**, *99*, 133.
(40) Deki, S.; Aoi, Y.; Hiroi, O.; Kajinami, A. *Chem. Lett.* **1996**, 433.

(41) Mintova, S.; Olson, N. H.; Valtchev, V.; Bein, T. *Science* **1999**, *283*, 958.
(42) Schefer, J.; McDaniel, R.; Schoenborn, B. P. *J. Phys. Chem.* **1988**, *92*, 729.
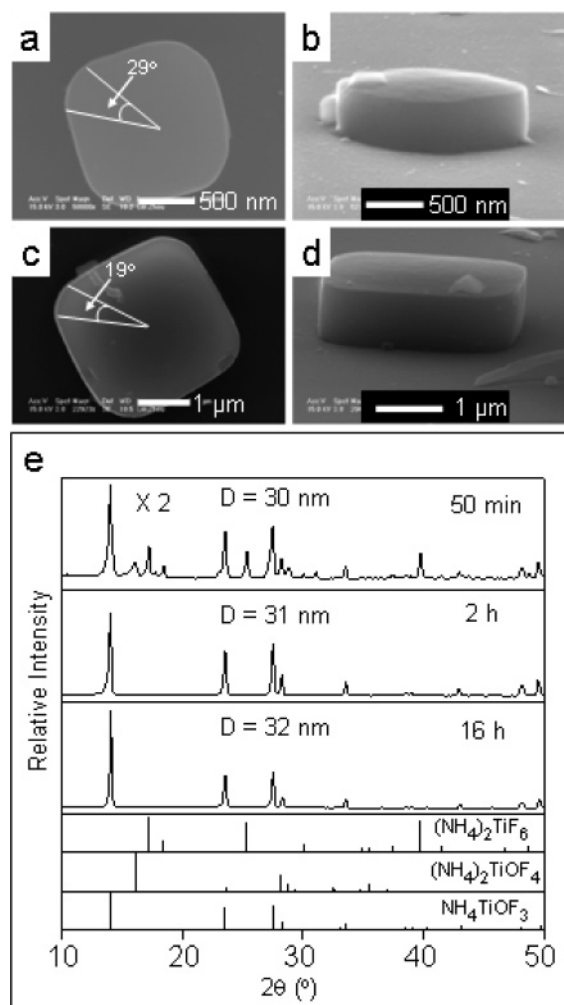
Figure 5. Top view and cross-sectional views of samples collected after reaction for (a and b) 2 h and (c and d) 8 h. The p-XRD patterns of samples collected after different reaction periods (e). ((NH₄)₂TiF₆ from JCPDS 73−2279; (NH₄)₂TiOF₄ from JCPDS 49−0161; NH₄TiOF₃ from ref 39.)

mesocrystal,[12] from the whole particle is shown in Figure 6b. The particle is presumably an intermediate formed during hydrolysis of (NH₄)₂TiF₆ to form NH₄TiOF₃. The precise identity is unclear, as there are many possible phases, e.g., $(NH_4)_xTiO_yF_z$ ($2y + z − x = 4$). Exampled representative equations can be written:

$$[TiF_6]^{2-} + 2H_2O \leftrightharpoons [Ti(OH)_2 F_4]^{2-} + 2HF \qquad (6)$$

$$[Ti(OH)_2 F_4]^{2-} \leftrightharpoons [TiOF_4]^{2-} + H_2O \qquad (7)$$

TEM samples for 30, 60, and 120 min were prepared with normally washed precipitates. TEM images of typical particles are shown in Figure 6c−e. The samples collected after different periods all have similar interior structures. As before, the SAED patterns show typical mesocrystal diffraction patterns ("single-crystal-like" diffraction with minor distortions), which could be indexed to NH₄TiOF₃. The HR-TEM images indicate that these particles are composed of nanocrystallites separated by interspaces/pores of size 2∼5 nm. The exterior shapes of these particles are significantly different. The particle collected after 30 min (Figure 6c) is cross or clover shaped. The particle collected after 60 min (Figure 6d) is an octagonal, with four
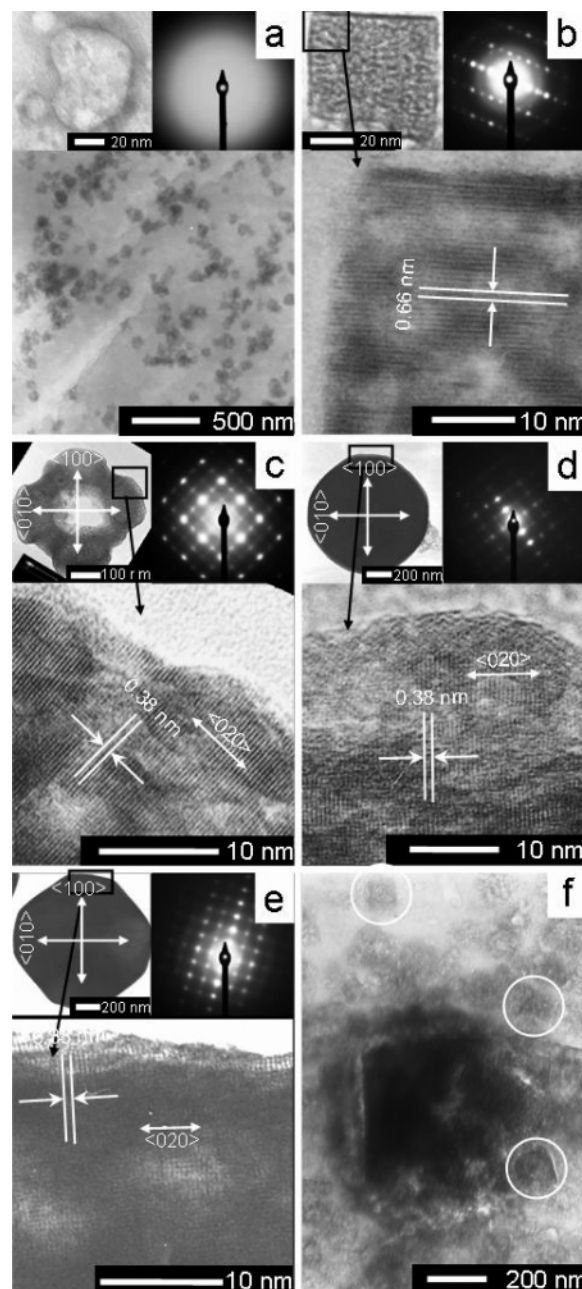

Figure 6. TEM images and SAED patterns of samples collected after different reaction times: (a) 5, (b) 20, (c) 30, (d) 60, (e) 120, and (f) 50 min. TEM samples for (a) 5, (b) 20, and (e) 50 are prepared from cloudy solutions. TEM samples for (c) 30, (d) 60, and (f) 120 min are prepared from washed precipitates.

sides that are slightly curved. The particles collected after 120 min (Figure 6e) have a larger size and more squarelike shape. The shape change as a function of time increasing indicates the likely crystal growth directions (i.e., ⟨100⟩ and ⟨010⟩ directions of NH₄TiOF₃), as confirmed by SEM investigations of the samples collected after 2 and 8 h (Figure 5a−d).

Figure 6f shows a particle collected after 50 min (reaction didn't complete, the TEM sample was prepared from a drop of cloudy solution). Small squarelike porous crystallites of dimensions between 60∼100 nm (indicated by circles) are visible everywhere around the center. This kind of porous crystallite has been observed in the 20 min sample and shown in Figure 6b, suggesting that the increased dimensions of the mesocrystal particles derive from controlled aggregation of smaller square-
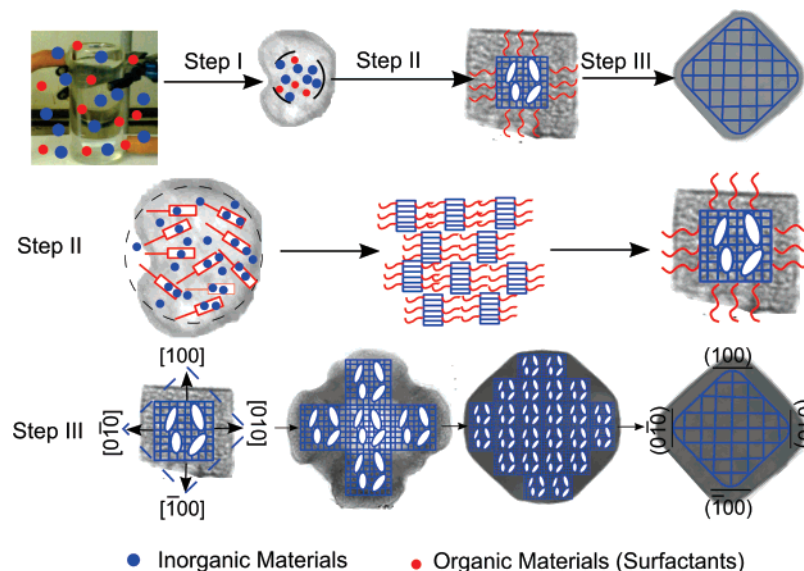
Figure 7. Schematic of crystal growth mechanism.

like porous nanocrystallites, rather than typical ion-by-ion growth processes.[12]

Mechanism of the Growth of the Mesocrystals. A mesocrystal growth mechanism can be tentatively proposed based on three steps: phase separation, matrix-mediated mesophase transformation (i.e., formation of primary building blocks), and self-assembly of the mesoscale building blocks. The schematic diagram is shown in Figure 7.

Under our experimental conditions, the surfactant concentration (23.08 wt %) is much higher than the critical micelle concentration (CMC, 0.0005 wt %) of Brij 58 ($C_{16}H_{33}(OCH_2$-$CH_2)_{20}OH$),[43] but not high enough for the initial solution to form any ordered mesophases (liquid crystal phase, such as cubic, hexagonal or lamellar phase).[44] The PEO functionalities (-$(OCH_2$-$CH_2)_n$) of the surfactant interact with titanium (IV) ions and/or condensed titanium-oxo species acting as Lewis base O-donors.[45,46] Condensation between these immobilized units leads the surfactants to coalesce and produce a new viscous phase dense in surfactant (step I). Similar phase-separation phenomena have been observed and discussed in preparation of mesoporous silica materials using low concentrations of surfactants.[47,48] Indeed a colloidal phase separation mechanism (CPSM)[48] has been proposed to explain the formation and morphology of rodlike SBA-15 materials. The difference between CPSM and the present work is that, after formation of a new phase, inorganic species presented in the viscous phase prefer to undergo crystallization via a "mesoscale-transformation",[14] rather than a true "liquid-crystal-templated" condensation that serves to preserve the order of the liquid crystal phases.

Possible transformation processes are illustrated in Figure 7 (step II). Cooperative reorganization of inorganic and organic components is important in the mesoscale transformation.[14] The

surfactant may act as a matrix for oriented crystallization of inorganic species. The layered structure of NH_4TiOF_3[39,49] (Figure S1, see the Supporting Information) is beneficial to this matrix-mediated nucleation. The surfactants can easily attach on the *ab* planes of NH_4TiOF_3. Nucleation of inorganic species causes the micelles of surfactants to unfold and form a highly uniform matrix. Figure 6b shows a "square" particle in which some wormlike spacing exists. Interaction between organic and inorganic species also hinders the hydrolysis of $(NH_4)_2TiF_6$ (eq 4 and 5) and leads to a high concentration of inorganic species ($(NH_4)_2TiF_6$ and H_3BO_3), which is beneficial to formation of NH_4TiOF_3 by virtue of higher levels of supersaturation.[40] In the transition of viscous microphases to primary "square" building blocks (step II), as the process of spontaneous self-assembly (or orientated attachment[37,50,51]) occurs rather than ion-by-ion attachment, boron-contained impurities remain in building blocks and serve to stabilize the porous crystal structure. The presence of boron-containing impurities has been indicated by elemental analysis (Table 1).

During step III, face-specific interactions between the building blocks lead to crystallographically ordered self-assembly. These building blocks become attached stepwise to the growing assembly of aligned building blocks and rotate to produce oriented nanocrystals (schematized in Figure 7 and proven by Figure 6f). The fusion of the blocks makes the original square borders of individual entities hard to see in resultant mesocrystals, but the interior pores are retained. It is apparent that the mesocrystal growth is a particle-by-particle (as reported elsewhere[12]) and not a classical ion-by-ion process. Moreover, the external morphology of mesocrystals is not a simple reflection of morphology of nanocrystalline building blocks. However, the formation mechanism of external facets in this work is similar to classical crystal growth mechanisms, in that the prominence of particular crystal faces in the final crystal shape or morphology is inversely proportional to the rate of growth of the face, i.e., the morphology of the crystal is defined

(43) Henderson, M. J.; Gibaud, A.; Bardeau, J. F.; White, J. W. *J. Mater. Chem.* **2006**, *16*, 2478.
(44) Mitchell, D. J.; Tiddy, G. J. T.; Waring, L.; Bostock, T.; McDonald, M. P. *J. Chem. Soc., Faraday Trans. 1* **1983**, *79*, 975.
(45) Soler-Illia, G. J. D. A. A.; Sanchez, C. *New J. Chem.* **2000**, *24*, 493.
(46) Soler-Illia, G. J. D. A. A.; Scolan, E.; Louis, A.; Albouy, P. A.; Sanchez, C. *New J. Chem.* **2001**, *25*, 156.
(47) Chan, H. B. S.; Budd, P. M.; Naylor, T. D. *J. Mater. Chem.* **2001**, *11*, 951.
(48) Yu, C. Z.; Fan, J.; Tian, B. Z.; Zhao, D. Y. *Chem. Mater.* **2004**, *16*, 889.

(49) Leblanc, M.; Ferey, G.; Depape, R.; Teillet, J. *Acta Crystallogr., Sect. C* **1985**, *41*, 657.
(50) Penn, R. L.; Banfield, J. F. *Geochim. Cosmochim. Acta* **1999**, *63*, 1549.
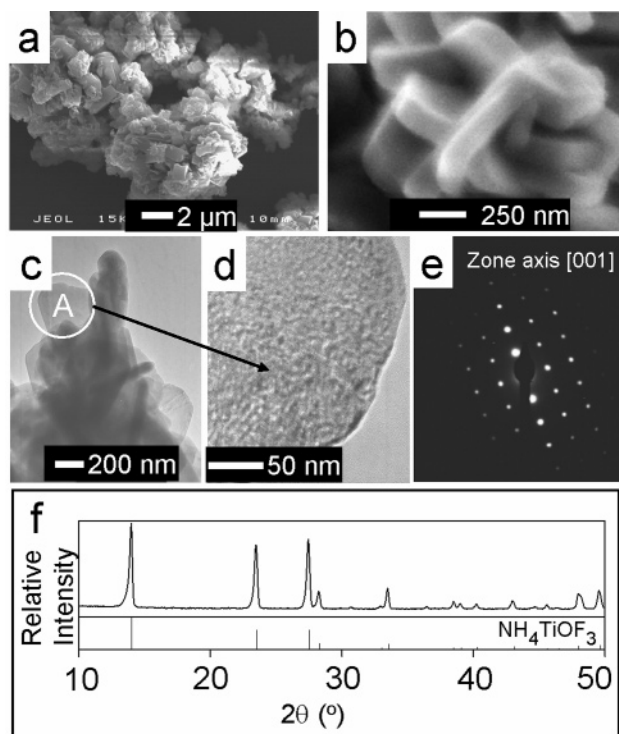(51) Penn, R. L.; Banfield, J. F. *Am. Mineral.* **1998**, *83*, 1077.

Figure 8. Results obtained from a sample prepared using continuous stirring: (a) low and (b) high magnification SEM images; (c) low and (d) high magnification TEM images; (e) SAED pattern and (f) p-XRD pattern of NH₄TiOF₃ materials. (Data for NH₄TiOF₃ are taken from ref 31.)

by the slowest growing faces.[52] The defining difference in our case is that much larger nanobuilding blocks substitute for atoms (ions). The results of TEM investigations (Figure 6) indicate that the anisotropy of the self-assembly originating from anisotropic adsorption of surfactant molecules resulted in faster crystal growth rates along $\langle 100\rangle/\langle 010\rangle$ directions for NH₄TiOF₃. As crystal growth proceeds, the (100), (010), ($\bar{1}$00), and (0$\bar{1}$0) facets diminish and corners form; the (110), ($\bar{1}$10), (1$\bar{1}$0), and ($\bar{1}\bar{1}$0) facets are enlarged and form edges (Figure 7).

To obtain further information concerning the effect of the reaction conditions on crystal growth processes and morphology of NH₄TiOF₃ mesocrystals, more work was carried out under similar conditions to those that were used to prepare a typical sample with Brij 58. In these investigations, a single parameter (from the method for the Brij 58 sample) was changed.

Effect of Stirring. SEM images of a sample prepared under the same conditions of those that were used to prepare a typical sample with Brij 58 but with extension of the stirring time beyond the initial period and into the course of the reaction are shown in Figure 8a and b. At high magnification, it is clear that the resultant large disordered aggregates (Figure 8a) are composed of smaller regular particles. Irregular TiO₂ aggregates that had been seen in typical samples prepared without surfactant or with Brij 56 (Figure 1a and Figure 2d) were not observed. The p-XRD pattern (Figure 8f) confirms that these aggregates are NH₄TiOF₃ and suggests that the continuous stirring influences the aggregation processes, and disrupts the oriented self-assembly process, changing the outer shape of the final product, not the chemical composition and/or phase.

TEM images of a sample prepared with continuous stirring are shown in Figure 8c−d. At low magnification (Figure 8c), an irregular aggregate is shown, notably different to the irregular aggregates in a typical sample prepared without surfactant (Figure 1b). These particles are clearly composed of smaller mesocrystallites (details are shown in Figure 8d). The corresponding SAED pattern (Figure 8e) for region A shows a single-crystal-like diffraction that can be indexed to NH₄TiOF₃ oriented along the [001] zone axis.

The agitation of bath solution markedly changes the morphology of the NH₄TiOF₃ mesocrystals. This effect is presumably achieved by disturbing the directed diffusion and aggregation of primary building blocks present in the unstirred solution.[53] The increased frequency and impact of particle collisions are likely to compete successfully with fluid shear forces[54] and hence lead to the random rather than directed assembly of NH₄-TiOF₃ particles. These effects will be stronger for the large particles than for the small ones, consistent with the observation that many large particles with regular shapes are characterized in the resultant aggregates.

Effect of Changing Reaction Temperature. Low magnification SEM images of samples prepared using identical conditions to those previously described in the Experimental Section for a typical sample prepared with Brij 58 (C₁₆H₃₃(OCH₂CH₂)₂₀-OH), but at reaction temperatures between 10 and 60 °C, are shown in Figure 9a−i. At temperatures of 10, 20, and 30 °C, discrete particles with a narrow size distribution and uniform shapes are obtained. Mean edge lengths and thicknesses of these samples were determined by SEM and are given in Table 2. Powder XRD results (Figure 9j) indicate these particles are crystalline NH₄TiOF₃. As the temperature increases from 10 to 30 °C, the mean edge length of the particles increases and the thickness decreases. Smaller curvature values for corners are observed (Figure 9a−f).

Higher reaction temperatures ($\geq$40 °C) lead to emergence of irregular particles (Figure 9g and h), which have similar morphologies with the anatase particles obtained in the typical sample prepared with Brij 56 (Figure 1b). Powder XRD patterns (Figure 9J) indicate they are polycrystalline anatase TiO₂. At 60 °C, NH₄TiOF₃ is rarely observed and anatase TiO₂ becomes the predominant phase (Figure 9h).

TEM images of the sample prepared at 10 °C are shown in Figure 9i, which suggests a porous mesocrystalline structure. The SAED pattern (inset) shows a single-crystal-like diffraction pattern that can be indexed to NH₄TiOF₃ along [001] zone axis. TEM investigations into the samples synthesized at 20−60 °C present similar results, i.e., the regular particles are NH₄TiOF₃ mesocrystals.

On the basis of the above investigation into morphology and composition, it is concluded that increasing the temperature enhances the formation of anatase. Higher temperatures increase the rates of the chemical processes and provide more energy to the system. Condensation between the immobilized metallic centers (Figure 7, step I) occurs more rapidly as the temperature is increased, as evidenced by more rapid onset of the clouding of the solution. Higher temperatures tend to promote hydrolysis and therefore impact on the mesophase transformation process

(52) Davey, R.; Garside, J. *From molecules to crystallizers: An introduction to crystallization*; Oxford University Press: London, 2000.

(53) Yu, S. H.; Cölfen, H.; Antonietti, M. *Chem.−Eur. J.* **2002**, *8*, 2937.
(54) Collier, A. P.; Hetherington, C. J. D.; Hounslow, M. J. *J. Crystal Growth* **2000**, *208*, 513.
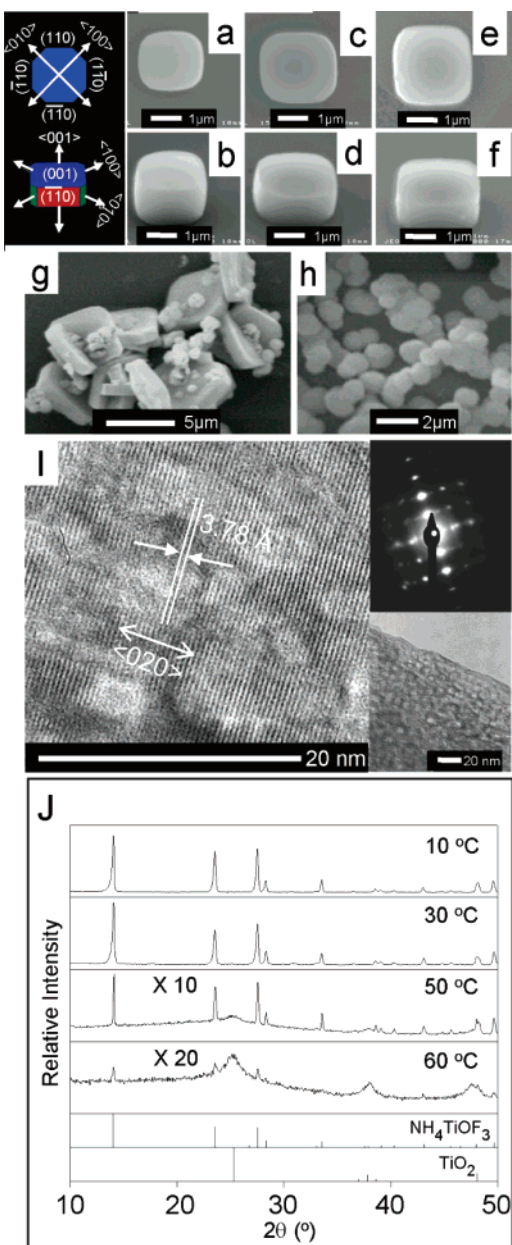
Figure 9. SEM images of samples prepared at 10 (a and b), 20 (c and d), 30 (e and f), 40 (g), and 60 °C (h); (i) TEM images and SAED pattern of the sample prepared at 10 °C; (j) p-XRD patterns of the samples prepared at various temperatures. (Data for TiO_2 taken from JCPDS 86−1156; NH_4-$TiOF_3$ from ref 39.)

Table 2. Mean Overall Edge Lengths of Samples Prepared between 10 and 35 °C and Corresponding Average Crystallite Sizes (D, Calculated Using the Scherrer Equation) Perpendicular to the (020) and (002) Planes (Denoted Using $D_{(020)}$ and $D_{(002)}$)

temp	mean overall edge lengths (μm)		average crystallite sizes (nm)	
(°C)	length/width	thickness	$D_{(020)}$	$D_{(002)}$
10	1.9(1)	1.7(2)	33	35
20	2.4(1)	1.3(1)	33	36
30	2.4(2)	1.2(1)	30	25
35	3.5(3)	0.78(9)	26	38

(Figure 7, Step II). As a result, some of nanocrystalline building blocks of NH_4TiOF_3 are completely converted to polycrystalline anatase instead of becoming involved in further self-assembly into mesocrystalline NH_4TiOF_3 (Figure 7, step III). This
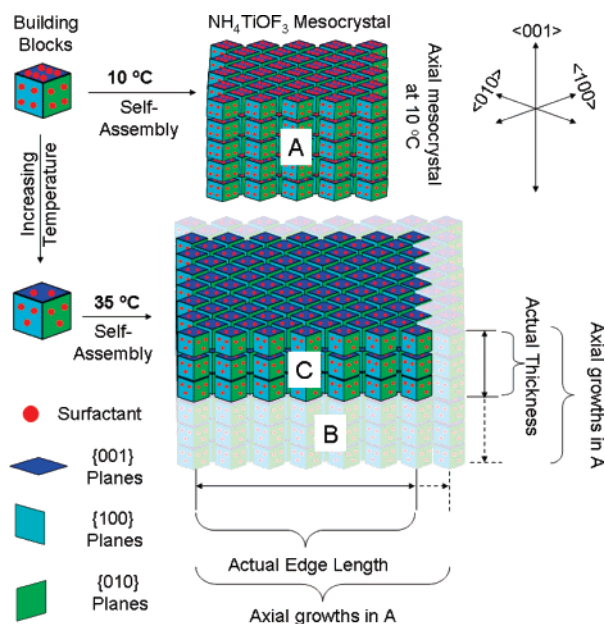
Figure 10. Illustrating the anisotropic effect of temperature on the growth of the mesocrystal.

suggestion is supported by the morphologies and compositions of the samples for 40, 50, and 60 °C (Figure 9g, h, and j).

At temperatures between 10 and 35 °C, the compositions of the samples are unchanged and only NH_4TiOF_3 mesocrystals are obtained. The major effect of changing the temperature is on the morphology, as provides a possibility to examine the impact of the temperature on the self-assembly process. A schematic diagram of the effect is given in Figure 10. For the self-assembly process of nanocrystalline building blocks (Figure 7, step III), increasing the temperature decreases the solution viscosity and increase mass transport. The nanocrystalline building blocks produced at higher temperatures have more chances to collide with the growing particle; hence larger average particle sizes are expected (visualized as mesocrystal B in Figure 10). SEM investigations (summarized in Table 2) indicate that as the temperature increases, though the edge lengths of the mesocrystals increases, the thickness does not increase but decrease. The anisotropy of mesocrystals is likely to originate from the preferential absorption of polyoxyethylene chains of surfactant molecules on {001} planes of the building blocks, which is presumably caused by the higher density of titanium atoms in the planes (Figure S1, see the Supporting Information). Increasing the temperature leads to a larger reduction in the number of PEO-moieties on {001} planes of nanocrystalline building blocks than that on other planes (schematized in Figure 10). The decrease of the thickness (i.e., length in {001} directions) is much greater than that of the edge length (Figure 10, mesocrystal B → C). Hence, the mesocrystals with longer edge lengths and thinner thicknesses are obtained at higher temperatures.

Effect of Changing the H_3BO_3 Concentration. Experiments were conducted using identical bath conditions to those described previously in the Experimental Section for a typical sample prepared with Brij 58 ($C_{16}H_{33}(OCH_2CH_2)_{20}OH$), but using different concentrations of boric acid (H_3BO_3). Solutions containing concentrations much lower than that for a typical sample (0.2 mol dm^{-3}), for example, 0.1 mol dm^{-3}, did not yield any precipitate even after being maintained at 35 °C for
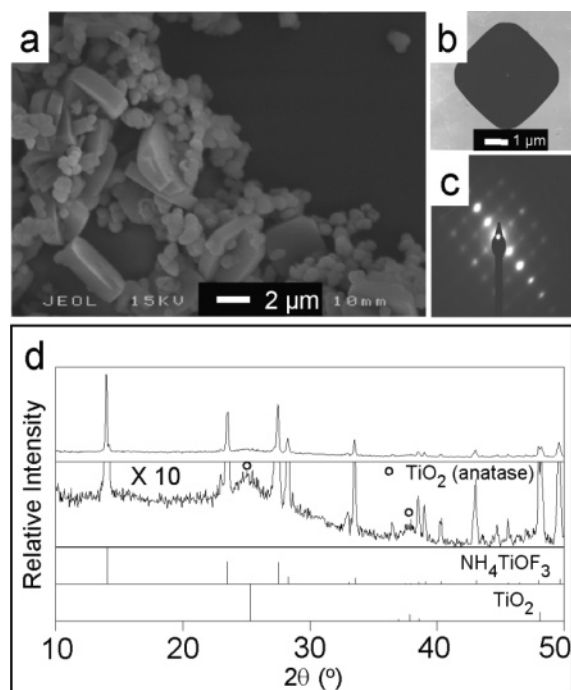
Figure 11. (a) SEM, (b) TEM, (c) SAED, and (d) p-XRD data collected from samples prepared in presence of 0.3 mol dm^{-3} H₃BO₃. (Data for TiO₂ taken from JCPDS 86−1156; NH₄TiOF₃ from ref 39.)

3 days, whereas H₃BO₃ concentrations much greater than 0.3 mol dm^{-3}, for example, 0.4 mol dm^{-3}, led to rapid precipitation before the surfactant was added. As 0.3 mol dm^{-3} H₃BO₃ was used, particles with similar morphologies to those synthesized at high temperatures (Figure 9g and h) are obtained (Figure 11a), suggesting a mixture of polycrystalline TiO₂ (anatase) and mesocrystalline NH₄TiOF₃, as confirmed by TEM (Figure 11b), SAED (Figure 11c), and p-XRD studies (Figure 11d). The shape of the NH₄TiOF₃ mesocrystals is very similar to that of a typical sample prepared with Brij 58 (Figure 4c).

On the basis of the above investigations into morphology and composition, it can be concluded that increasing the concentration of H₃BO₃ leads to formation of both nanocrystalline anatase TiO₂ and mesocrystalline NH₄TiOF₃. The morphology of the latter remains largely similar to a typical sample prepared with Brij 58. In the context of "building block" formation (Figure 7, steps I and II), increased concentration of H₃BO₃ may be thought to accelerate the removal of F$^-$ and consequently drive further hydrolysis of [Ti(OH)₃F₃]$^{2-}$ (eq 4). The hydrolysis process may then proceed to completion and produce [Ti(OH)₆]$^{2-}$ and ultimately lead to formation of nanocrystalline TiO₂ (eq 2). During the conversion process from amorphous to crystalline material, a portion of the viscous phases (Figure 7, step I) may undergo complete hydrolysis to yield TiO₂, while the bulk of the viscous phases partially hydrolyze and "transform" to the nanocrystallite building blocks for NH₄TiOF₃ (Figure 7, step II). High concentrations of boric acid do not appear to significantly perturb the self-assembly processes governing the directed aggregation of preformed NH₄TiOF₃ nanocrystalline building blocks.

Effect of Changing Surfactant Concentration. A series of experiments were conducted using identical reaction conditions to those previous described in the Experimental Section for a typical sample prepared with Brij 58 (C₁₆H₃₃(OCH₂CH₂)₂₀OH), but using different Brij 58 concentrations (0.99∼16.67 wt %).
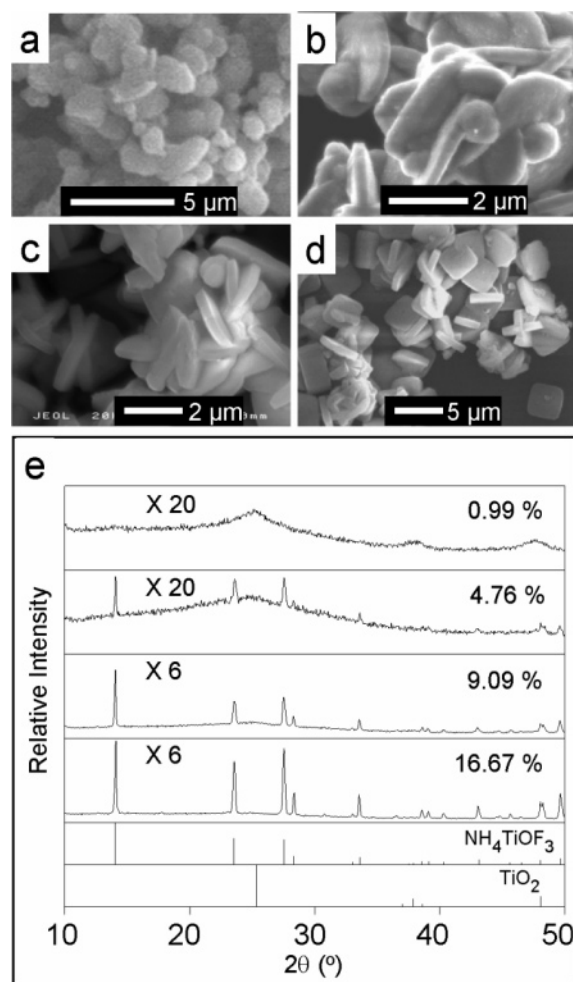

Figure 12. SEM images of samples prepared with different surfactant concentration: (a) 0.99%, (b) 4.76%, (c) 9.09%, and (d) 16.67%. (e) The p-XRD patterns of these samples. (Data for TiO₂ taken from JCPDS 86−1156; NH₄TiOF₃ from ref 39.)

As with the typical sample, the surfactant concentrations are much higher than the critical micelle concentration (CMC, 0.0005 wt %) of Brij 58,[43] but lower than that at which ordered mesophases are formed.[44] The solutions in this series experiment are likely to form surfactant micelles, but no ordered mesophases should be formed.

SEM images of the resultant samples are shown in Figure 12a−d. At a Brij 58 concentration of 0.99 wt % or 1.96 wt %, precipitates formed as irregular aggregates of TiO₂ nanocrystallites. At concentration above 16.67 wt % (which are still below the concentrations at which an ordered mesophase formed), an abrupt disappearance of irregular aggregates is apparent. Moreover, increasing surfactant concentration tends to separate and isolate discrete mesocrystals. Finally, at a threshold concentration of 23.08 wt % (at which the typical sample were prepared), only regular particles appear to be formed (Figure 2b). Detailed information on the morphologies of individual mesocrystalline particles is shown in Figure S2 (see the Supporting Information).

Diffraction patterns for the samples are shown in Figure 12e. As the surfactant concentration increases, the NH₄TiOF₃ phase appears and progressively becomes the dominant product. Amounts of anatase diminish gradually as surfactants are increased, and it is no longer present above 16.67 wt %.
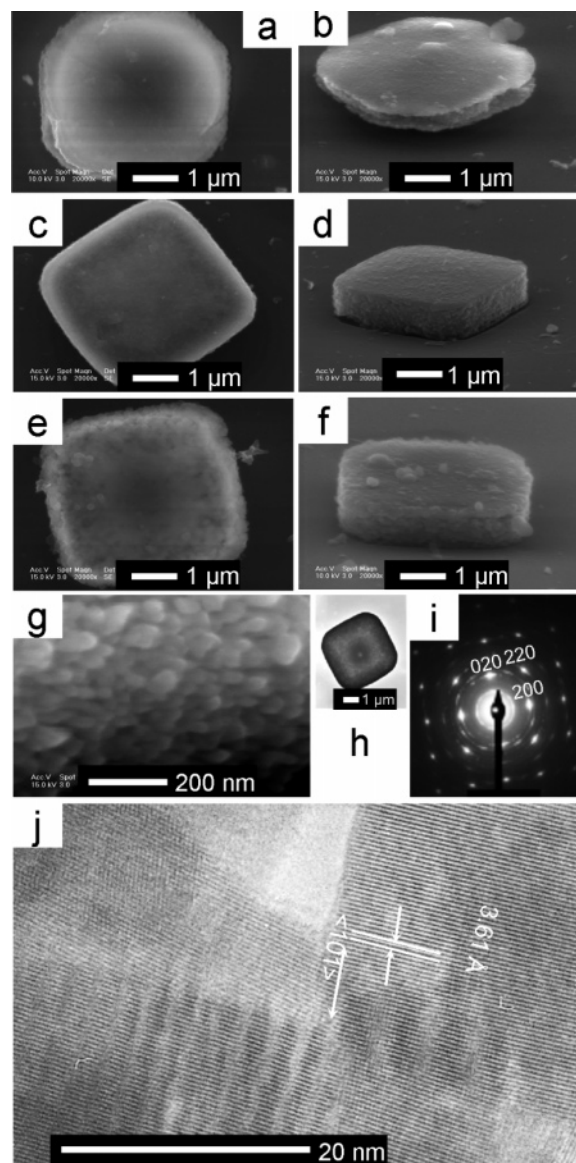
Figure 13. Top view and cross-sectional view SEM images of heat-treated samples that are originally prepared with (a and b) Brij 56, (c and d) Brij 58, or (e and f) Brij 700. (g) High magnification SEM and (h) low and (j) high magnification TEM images of the heat-treated sample with Brij 58; (i) SAED pattern of the heated Brij 58 sample.

In summary, the surfactant concentration has a marked and defined effect on the composition and morphology of products. Both the stability of hydrolyzed intermediates and the ability of surfactant-stabilized building blocks to self-assemble into larger mesocrystals are sensitive to the initial concentration of surfactant in solution. Very low concentration of surfactant leads to rapid and complete hydrolysis of precursors to anatase TiO_2, whereas higher concentrations tend to lead to increasing formation of discrete NH_4TiOF_3 nanocrystals that undergo a self-assembly process to form larger mesocrystals. Higher concentrations increase the viscosity of the solutions and therefore decrease the mobility of mesocrystals. Fewer collisions between the incomplete mesocrystals may happen. Irregular aggregates of mesocrystals are the major form of the product at low surfactant concentrations but are seldom found in the samples that are synthesized at high surfactant concentrations.

Oriented Transformation of NH_4TiOF_3 Mesocrystals to TiO_2 Mesocrystals by Thermal Treatment. There are remark-
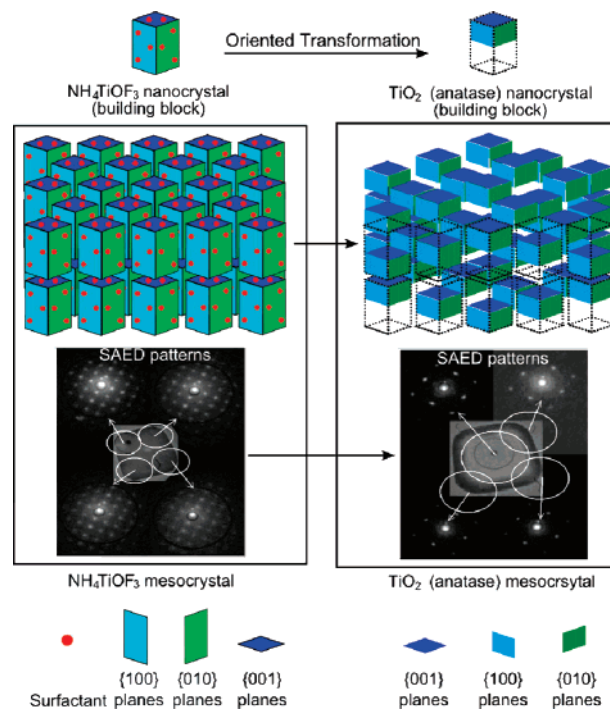

Figure 14. Illustration of the oriented transformation of NH_4TiOF_3 mesocrsytal to TiO_2 (anatase) mesocrystal.

able similarities between the known anatase structures and that which has been deduced for NH_4TiOF_3. Titanium atoms' positions in the [001] planes are similar in both structures, but in NH_4TiOF_3, these are separated by ammonium in a lamellar structure (crystal structures of anatase and NH_4TiOF_3 are shown in Figure S1 in the Supporting Information). Hence it is not surprising that themolysis can lead to an oriented transformation from NH_4TiOF_3 to anatase.

SEM investigations indicate that after heat-treatment, the overall shapes of NH_4TiOF_3 mesocrystals are preserved, although in all cases there is an apparent roughening of the previously smooth facets and visible porosity in the final structure. SEM images of heat-treated samples are shown in Figure 13a−f. The mean edge length and thickness of heat-treated NH_4TiOF_3 mesocrystals are very similar to the virgin samples. For a typical sample prepared with Brij 58, after heat-treatment, values of 3.5 (3) and 0.8(1) μm were obtained (cf. 3.5(3) and 0.78(9) μm initially). High magnification SEM images shown in Figure 13g provide further details of nanocrystallites that comprise the heat-treated mesocrystals. The dimension of these primary particles appears to be in the range 20∼40 nm.

The p-XRD patterns obtained from heated samples are shown in Figure S3 (for details see Supporting Information) and indicate that after heat-treatment at 450 °C for 2 h, all as-prepared samples are converted to TiO_2 (anatase). The average crystallite sizes of the heat-treated samples were determined: 24 nm (D_{200}) and 14 nm (D_{004}) for the typical sample prepared with Brij 58; 27 nm (D_{200}) and 16 nm (D_{004}) for the typical sample prepared with Brij 700. The two samples exhibited measurable changes in dimensions along the $\langle 001 \rangle$ directions, but almost no change along the $\langle 100 \rangle$ and $\langle 010 \rangle$ directions. The contraction along the $\langle 001 \rangle$ directions is due to the collapse of the lamellar structures of NH_4TiOF_3 to more compacted anatase TiO_2. The SAED pattern (Figure 13i) depicts

Table 3. TGA Data Collected for Typical Samples Prepared with Brij 56, Brij 58, or Brij 700 at a Heating Rate of 5 °C min⁻¹ in Air

surfactants used	weight loss (%)[a]				
Brij 56	6.97 (25∼237 °C)	18.91 (237∼366 °C)		6.64 (366∼454 °C)	
Brij 58	1.43 (25∼245 °C)	12.84 (246∼310 °C)	14.50 (310∼361 °C)	5.53 (361∼424 °C)	12.60 (424∼458 °C)
Brij 700	1.90 (25∼243 °C)	12.37 (243∼316 °C)	14.04 (316∼360 °C)	4.35 (360∼421 °C)	18.24 (421∼470 °C)

[a] Mass loss steps can be attributed the following processes. Phase: $NH_4TiOF_3 \rightarrow HTiOF_3 \rightarrow TiOF_2 \rightarrow TiO_2$; mass loss: 12.2%, 14.4%, 15.8%, respectively.

a representative mesocrystal diffraction pattern[12] (single-crystal-like diffraction with minor distortions), confirming that these particles are also mesocrystalline in nature but of TiO_2 (anatase). Further information on the mesocrystal substructure was gained from HR-TEM data (Figure 13j). After heat-treatment, nanocrystals with a size of 20∼30 nm are apparent, consistent with SEM results (Figure 13g). As noted previously,[16] identical diffraction patterns were obtained across the entire mesocrystal held in static orientation and moved in the microscope in diffraction mode, entirely consistent with mesocrystal assemblies comprising crystallographically aligned nanocrystals (shown in Figure 14).

To understand better the thermal conversion process, thermogravimetric (TGA) studies were performed. The results are summarized in Table 3. For the typical samples prepared with Brij 58 or Brij 700, a comparison with theoretical mass loss values (calculated by assuming the processes shown in Table 3) leads to the conclusion that the conversion process from NH_4TiOF_3 to TiO_2 is tentatively composed of five sequential steps. In the first stage (25∼242 °C), impurities such as water and other volatiles are removed. In the second step (242∼316 °C), NH_4TiOF_3 is converted to $HTiOF_3$ upon removal of NH_3. In the third step (316∼354 °C), $HTiOF_3$ is converted to $TiOF_2$ with loss of HF. In the penultimate step (360 and 420 °C), B-containing impurities appear to be decomposed or removed. Finally (420∼470 °C) $TiOF_2$ is converted to TiO_2. The TGA data of a typical sample prepared with Brij 56 differed from those with Brij 58 or Brij 700, owing to the nature of the starting material (i.e., a mix of anatase TiO_2 and mesocrystalline NH_4TiOF_3). The presence of TiO_2 led to only three apparent steps instead of the five mass loss steps.

The critical parameters are $a = 7.5594$ Å, $b = 7.5754$ Å, $c = 12.7548$ Å for NH_4TiOF_3 and $a = b = 3.7845$ Å, $c = 9.5143$ Å for anatase TiO_2. The {001} planes (i.e., *ab* planes) are similar in the two compounds with an average lattice mismatch of only 0.02% (crystal structures of anatase and NH_4TiOF_3 are shown in Figure S1 in the Supporting Information). Moreover, titanium atoms in the {001} planes have a very similar arrangement in both materials. During the thermal phase transformation, NH_4TiOF_3 can serve as a lattice-matched substrate, as well as a source of all titanium and some of the oxide ions. Because of the restricted dimensions and low surface interfacial energies, small TiO_2 grains may generate and, crucially, remain with the same orientation as the precursor NH_4TiOF_3. Further oriented nucleation of TiO_2 is promoted via these small grains to develop larger grains and consume NH_4TiOF_3. Along the ⟨001⟩ directions, TiO_2 has greater atom density, and thus contraction is expected. In the present study, this change in dimensions of individual primary nanocrystallites has been observed in SEM images and further evidenced through p-XRD data. We believe this oriented transformation (from NH_4TiO_3 to anatase) which

happened on the individual primary nanocrystallites is a topotactic transformation[55] (illustrated in Figure 14). The SAED patterns shown in Figure 14 give more evidence of the crystallographically equivalent and orientational relationship between two materials on the {001} planes. The original dimensions of NH_4TiOF_3 mesocrystals are largely retained after thermal treatment; no contraction of structure occurs after thermal treatment. This interesting phenomenon derives from the unusual internal structure of mesocrystals, which are composed of smaller nanocrystallites. An illustration of the oriented transformation is shown in Figure 14.

Oriented Transformation of NH_4TiOF_3 Mesocrystals to TiO_2 Mesocrystals by Washing with H_3BO_3 Solution. Topotactic conversions[56] are recently well discussed in thermal reactions of solids. One similar solution-mediated topotactic structural transformation was reported by Feng et al. in hydrothermal conversion of $H_{1.08}Ti_{1.73}O_4$ to $BaTiO_3$ using a 0.1 mol dm⁻³ $Ba(OH)_2$ solution.[57] In the work, Ba^{2+} ions "migrate into the crystal bulk through the interlayer pathway and react with the TiO_6 octahedral layers of $H_{1.08}Ti_{1.73}O_4$ in the crystal bulk to form $BaTiO_3$ in situ".

In the present work, boric acid (H_3BO_3, 0.5 mol dm⁻³) solution was reacted with NH_4TiOF_3 mesocrystals (i.e., the sample prepared with Brij 58 under the typical reaction conditions which have been given in the Experimental Section) to effect conversion to anatase. The reaction can be summarized as

$$4NH_4TiOF_3 + 3H_3BO_3 \rightleftarrows 4NH_4^+ + 3BF_4^- + OH^- + 4H_2O + 4TiO_2 \downarrow (anatase) \quad (eq\ 8)$$
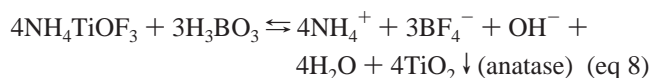
Formation of the anatase involves the dissolution of ammonium and fluoride ions from the NH_4TiOF_3 mesocrystals, followed by collapse to anatase. Results indicated that complete conversion of NH_4TiOF_3 mesocrystals to anatase is achieved after reacting at 35 °C for 4 h (Figure 15g). The average crystallite size, estimated after complete conversion, using the Scherrer Equation, was 6 nm. Increasing the solution temperature reduced the required time for a complete conversion, e.g., at 60 °C, only 2 h were needed (Figure 15g), and the average crystallite size is apparently increased to 8 nm. At both temperatures, the average crystallite sizes are much smaller than those for untreated or heat-treated samples because the H_3BO_3-treatment appears to fragment the original NH_4TiOF_3 nanoparticles due to dissolution and disaggregation of some materials' recrystallization. The most obvious consequence of reduction in nanoc-

(55) Clark, J. B.; Hastie, J. W.; Kihlborg, L. H. E.; Metselaar, R.; Thackeray, M. M. *Pure Appl. Chem.* **1994**, *66*, 577.
(56) Figlarz, M.; Gérand, B.; Delahayevidal, A.; Dumont, B.; Harb, F.; Coucou, A.; Fievet, F. *Solid State Ion.* **1990**, *43*, 143.
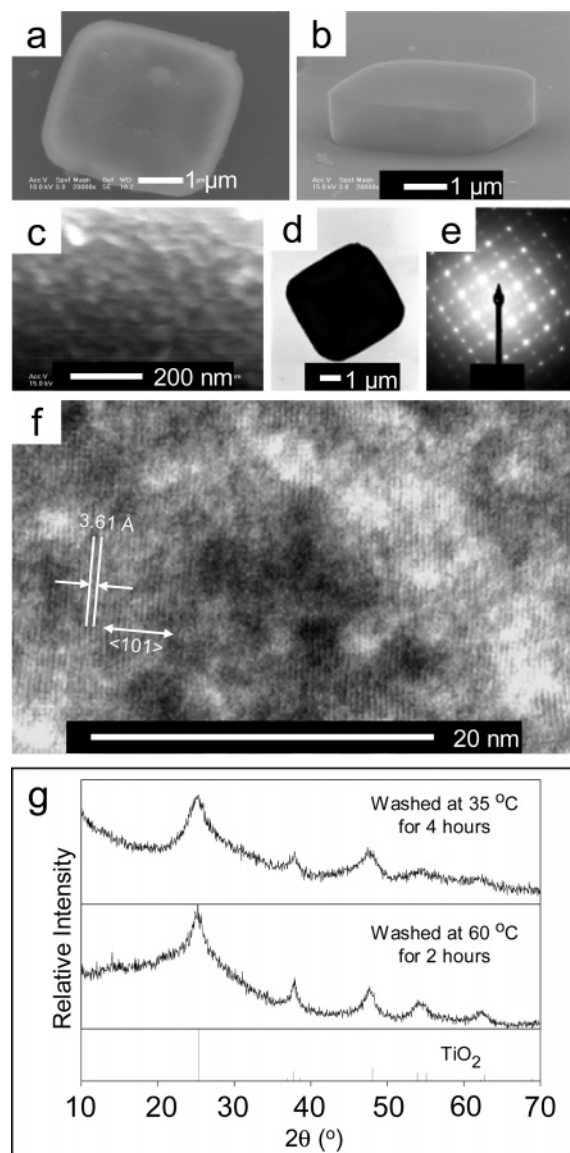(57) Feng, Q.; Kajiyoshi, K.; Yanagisawa, K. *Chem. Lett.* **2003**, *32*, 48.

Figure 15. (a) Top, (b) cross sectional, and (c) high magnification SEM images of a sample washed with 0.5 mol dm^{-3} H$_3$BO$_3$ at 35 °C for 4 h. (d) Low magnification TEM image, (e) SAED pattern, and (f) high magnification TEM image of the sample washed with 0.5 mol dm^{-3} H$_3$BO$_3$ at 60 °C for 2 h. (g) The p-XRD patterns obtained from both samples (reference TiO$_2$ data from JCPDS 86−1156).

rystallite size is the broadening of diffraction reflections (Figure 15 g). SEM images of the H$_3$BO$_3$-treated sample (Figure 15a and b) indicate that the overall shape of NH$_4$TiOF$_3$ mesocrystals is preserved after H$_3$BO$_3$-treatment. A high magnification SEM image of the sample washed at 35 °C for 4 h is shown in Figure 15c.

TEM images and SAED pattern of a sample washed with 0.5 mol dm^{-3} H$_3$BO$_3$ solution at 60 °C are shown in Figure 15d−f. The results were consistent with complete conversion to anatase TiO$_2$. The primary nanocrystallites are aligned to form

larger particles and ultimately anatase mesocrystals (Figure 15f). The overall SAED pattern is similar to those obtained for heated samples. The main difference is that the H$_3$BO$_3$-washed materials are composed of smaller nanocrystals than the heat-treated samples, as is suggested by microscopy (Figure 15f) and p-XRD data (Figure 15g). Moreover, the SAED pattern of the material (15e) typically presents diffraction patterns associated with anatase mesocrystals (single-crystal-like with minor distortions).

Conclusions

A facile method has been developed to synthesize mesocrystals of NH$_4$TiOF$_3$. The factors that affect the growth of NH$_4$-TiOF$_3$ mesocrystals have been studied including mass transport (rate of stirring of reaction solutions, viscosity of solutions), reaction temperature, and reagent concentrations. Uniform size distributions were obtained over a wide range of temperatures (between 5 and 35 °C). The shapes of NH$_4$TiOF$_3$ mesocrystals can be varied from tabular to more elongated octagonal prismatic by tuning the reaction temperature. The surfactant plays an important role in both the controlling hydrolysis of (NH$_4$)$_2$TiF$_6$ and the self-assembly processes. The former determines the chemical composition of final products; the latter directs the shape of final mesocrystalline particles.

A potential use for the NH$_4$TiOF$_3$ mesocrystals has been demonstrated. By thermal decomposition or aqueous hydrolysis with H$_3$BO$_3$, the mesocrystals of NH$_4$TiOF$_3$ orientatedly transform to anatase mesocrystals. The product broadly maintains similar dimensions and shape to the precursor NH$_4$TiOF$_3$ material. It seems likely that the similarities in crystal structures of NH$_4$TiOF$_3$ and TiO$_2$ provide the possibility for the oriented transformation. During such transformation, the NH$_4$TiOF$_3$ mesocrystal provides a crystallographically matched template for the subsequent growth of the TiO$_2$ mesocrystals. The use of the crystallographically matched and chemically related crystalline NH$_4$TiOF$_3$ mesocrystals circumvents problems associated with amorphous-crystalline transitions, which hinder conventional routes to mesostructured metal oxides. The preparation of anatase in a completely new form, as mesocrystals, is of academic and potentially industrial interest, for example, for use in dye sensitized solar cells (DSSCs). In principle, this kind of oriented conversion can be applied to other materials, the prerequisite being that the precursor material and resultant product are a good crystallographic match.

Supporting Information Available: Crystal structures, additional SEM images, and p-XRD patterns. This material is available free of charge via the Internet at http://pubs.acs.org.

JA076187C